

Energy Sources, Part A: Recovery, Utilization, and Environmental Effects

ISSN: (Print) (Online) Journal homepage: <https://www.tandfonline.com/loi/ueso20>

A new virtual oscillator control for synchronization of single-phase parallel inverters in islanded microgrid

Vikash Gurugubelli, Arnab Ghosh & Anup Kumar Panda

To cite this article: Vikash Gurugubelli, Arnab Ghosh & Anup Kumar Panda (2022) A new virtual oscillator control for synchronization of single-phase parallel inverters in islanded microgrid, Energy Sources, Part A: Recovery, Utilization, and Environmental Effects, 44:4, 8842-8859, DOI: [10.1080/15567036.2022.2126560](https://doi.org/10.1080/15567036.2022.2126560)

To link to this article: <https://doi.org/10.1080/15567036.2022.2126560>



Published online: 21 Sep 2022.



Submit your article to this journal



Article views: 166



View related articles



View Crossmark data



Citing articles: 6 View citing articles



A new virtual oscillator control for synchronization of single-phase parallel inverters in islanded microgrid

Vikash Gurugubelli, Arnab Ghosh, and Anup Kumar Panda

Department of Electrical Engineering, National Institute of Technology Rourkela, Rourkela, Odisha, India

ABSTRACT

This paper describes the concept of virtual oscillator control (VOC) for parallel-connected single-phase inverters (SPIs). The principal idea is to introduce a series of weakly coupled oscillators (Deadzone oscillator-based VOC and Van der Pol oscillator-based VOC) that can be used for the regulation of single-phase power inverters in an islanded microgrid (MG). Its dynamic equations are used to provide the frequency and amplitude references of the inverters. In these traditional methods, there is always the presence of a 3rd order harmonic in the output voltage, which causes a significant amount of 3rd order harmonic current in the system. The non-linear dynamical equations of the oscillator are analyzed and its non-linear current source (NCS) is made simpler in order to develop new VOC for SPIs that can effectively get rid of the 3rd order harmonic component in the oscillator's output voltage. Finally, an extensive comparison of Deadzone-based VOC (Dz-VOC), Van der pol-based VOC (VdP-VOC), and new VOC-based controllers with linear and nonlinear loads is presented. The new VOC-based controller minimizes the 3-order harmonic component in the output voltage and achieves a quicker response compared to the conventional VdP-VOC-based controller. Simulation results of the Dz-VOC, VdP-VOC, and proposed new VOC-based control methods with different loads (Resistive, Linear RLC, non-linear) were compared and analyzed in detail. The total harmonic distortion (THD) of the current in Dz-VOC, VdP-VOC, and new VOC are 1.98%, 1.11%, and 0.21%, respectively. The 3rd harmonic is dominant in both Dz and VdP VOCs, while in the new VOC the 3rd harmonic is very less and below 0.1%. The new VOC is also showing good current sharing and fast voltage synchronization (within 0.2 s). Hardware experimentation is also carried out to analyze the efficacy of the proposed new VOC controlled SPI in standalone MG. The results clearly depict that the new VOC control strategy is quite efficient in handling the output voltage harmonics and situations of different loadings in the standalone MG.

ARTICLE HISTORY

Received 4 November 2021

Revised 13 September 2022

Accepted 14 September 2022

KEYWORDS

virtual oscillator control;
deadzone VOC; van der pol
VOC; parallel inverters;
islanded microgrid

Introduction

Power converters are an important part of microgrid (MG) systems because they are the link between power sources and the utility grid. The functions of the power converters are power conversion, stabilizing the output voltage and frequency, improving the quality of the power, and making sure that the power is running as efficiently as possible [Rocabert et al. 2012, Guerrero et al. 2013]. The parallel operation of converters is an essential part of an MG. Synchronization and power sharing are the most important goals for MG control. Droop control is the most common type of decentralized control for inverters in islanding MGs. This well-known method does not require any communication and is based on the synchronous generator in a conventional grid. Droop control is a method that shows

a linear relationship between the frequency and voltage amplitude of the inverter and the active and reactive power outputs [Rocabert et al. 2012, Zhong and Weiss 2011]. Even though there are several improved approaches, the disadvantages are still evident [Guerrero et al. 2013], such as slow dynamic response caused by the low pass filter (LPF), an ineffective way of power sharing, poor performance with line impedance, and nonlinear loads, etc.

Virtual synchronous machine techniques are focused on the direct simulation of machine dynamics [De Brabandere et al. 2007, Liu et al. 2017]. Virtual oscillator control (VOC), which differs from machine-inspired methods, is a control system in which inverters are designed to emulate the dynamics of nonlinear oscillators like Dz and VdP VOCs [Johnson et al. 2014, Johnson et al. 2016]. The idea of interconnected nonlinear oscillators, which have been utilized to represent various synchronization phenomena in physical and biological systems [Strogatz 2012], serves as the foundation for this method. These inverters, which are controlled by a VOC, can produce self-sustained periodic voltages, power sharing without communication, as well as the capability to regulate both voltage and frequency. Inverter time-domain oscillator controls were first developed in [Törres, Hespanha, and Moehlis 2012]. VOC can respond more quickly than traditional droop control approaches. VOC controlled single-phase and three-phase island MG is presented successfully in [Dhople, Johnson, and Hamadeh 2013]. According to [Hansen, Breyer, and Lund 2019], the VOC in the island mode can achieve global asymptotic synchronization. The analysis in [Johnson et al. 2014] and [Dhople et al. 2014] shows that the waveforms produced by the Dz-VOC and VdP-VOC implementations are similar, but the VdP-VOC form is easier to model mathematically. The analysis in [Johnson et al. 2016] showed how the voltage and frequency of the VdP-VOC can be controlled, and it also described a complete design process that meets user defined performance requirements. The analysis also showed that, in a steady state, the VdP-VOC has the same functions as droop control, but its time-domain implementation gives it a faster dynamic speed [Sinha et al. 2017]. There have been more comparisons between VdP-VOC and traditional droop control in [Johnson et al. 2017]. In [Raisz, Thai, and Monti 2019, Awal et al. 2020], a hierarchical arrangement was presented. In this structure, the VdP-VOC was given an extra outer loop that controls the power flow. In [Lu et al. 2019], the VdP-VOC was changed so that it could be used in applications with fast acting analog inner current control loops. In [Awal et al. 2020], a way for grid-connected inverters to reject current harmonics selectively was shown. [Lu, Dutta, and Johnson 2022] show how VdP-VOC can be used to synchronize inverters that are connected in parallel. In [Luo et al. 2021], a new VOC presented for inverters to get rid of the traditional Vdp-VOC 3rd harmonic voltage without changing the way it drops. When compared to the conventional VdP-VOC [Johnson et al. 2016], the new VOC-based inverters can respond much more quickly. Compared to the conventional VdP-VOC [Awal et al. 2020], the suggested new VOC can effectively nullify the 3rd harmonic without affecting the system performance. This new VOC method is applied to a 3-phase grid-tied inverter system. In [Luo et al. 2022], a Kalman-filter is used to nullify the harmonic current in VOC controlled grid-tied inverter.

In this work, the authors applied Dz-VOC and VdP-VOC control methods for controlling the single-phase parallel inverters operated in islanded MG. In these traditional methods, there is always a 3-order harmonic in the output voltage, which reasons a significant amount of 3-order harmonic current in the system. In this, the nonlinear dynamical equations of the oscillator are analyzed and its NCS is made simpler. This is done to come up with a new VOC for SPIs that can effectively get rid of the 3rd order harmonic in the oscillator's output voltage. Figure 1 shows the system under consideration in this study. A standalone MG is created by connecting three single-phase inverters in parallel.

The following is an outline of the significant contributions made by this work:

- (a) Implementation of the proposed new VOC and two well-known conventional VOC methods for synchronization of parallel SPIs in islanded MG. The proposed new VOC method is the first time used for the SPIs.

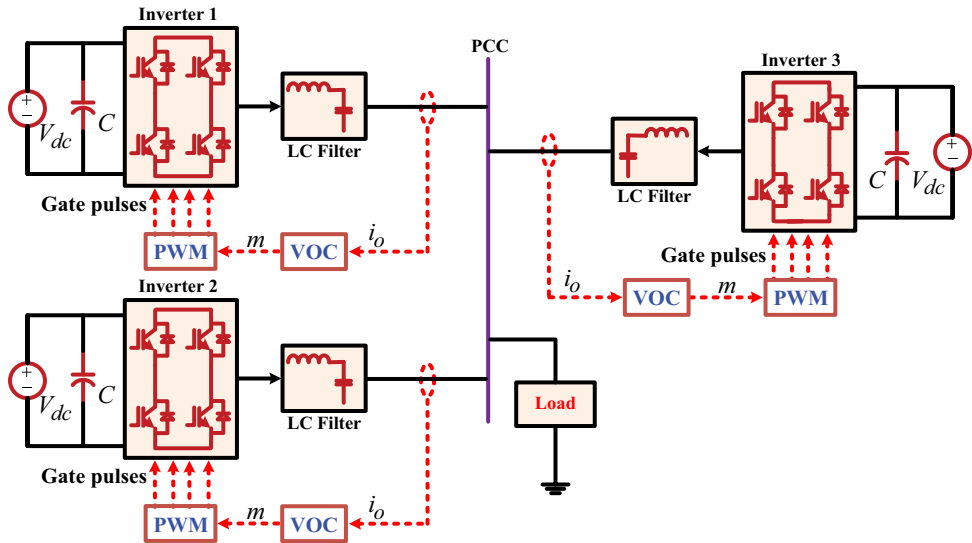


Figure 1. Single-Phase parallel inverter system.

- (b) The proposed new VOC nonlinear dynamical equations are analyzed, and its NCS is made simpler. A computational analysis of the new VOC is also given, to eliminate the 3rd order harmonic component in the output voltage.
- (c) Simulation results of the Dz-VOC, VdP-VOC, and proposed new VOC-based control methods with different loads (Resistive, Linear RLC, non-linear) were compared in detail.
- (d) Hardware experimentation is being tested on the proposed new VOC controlled SPI in standalone MG. A resistive load (which may vary between 27 and 54 Ω) is used in the experimentation.

Control structures

The VOC provides a decentralized control mechanism that can be used for islanded MGs. With this method, inverters are regulated to imitate the dynamics of non-linear oscillators. The magnitude and frequency of the inverter output voltage are also under the VOC's control. Because of this, the inverter output voltages have been synchronized with one another. This strategy ensures that the load power is distributed in harmony with the power ratings of the inverters while also avoiding any communication between the inverters.

Deadzone oscillator based VOC

Dz-VOC is dependent on the Dz function $f(v_{osc})$, as defined below:

$$f(v_{osc}) = \begin{cases} 2\sigma(v_{osc} - \varphi), & v_{osc} > \varphi \\ 0, & |v_{osc}| \leq \varphi \\ 2\sigma(v_{osc} + \varphi), & v_{osc} < -\varphi \end{cases} \quad (1)$$

where v_{osc} denotes the Dz-VOC terminal voltage, φ is the offset voltage, and σ is the slope of the voltage dependent current source (VDCS) function $g(v_{osc})$, it is represented as

$$g(v_{osc}) = f(v_{osc}) - \sigma v \quad (2)$$

The functions $f(v_{osc})$ and $g(v_{osc})$ are shown in Figure 2(a, b), correspondingly.

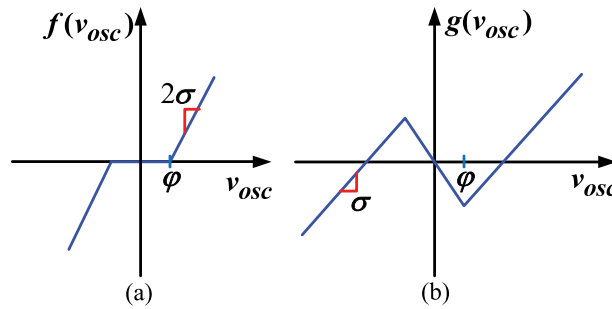


Figure 2. (a) Dz function characteristics (b) VDCS function characteristics.

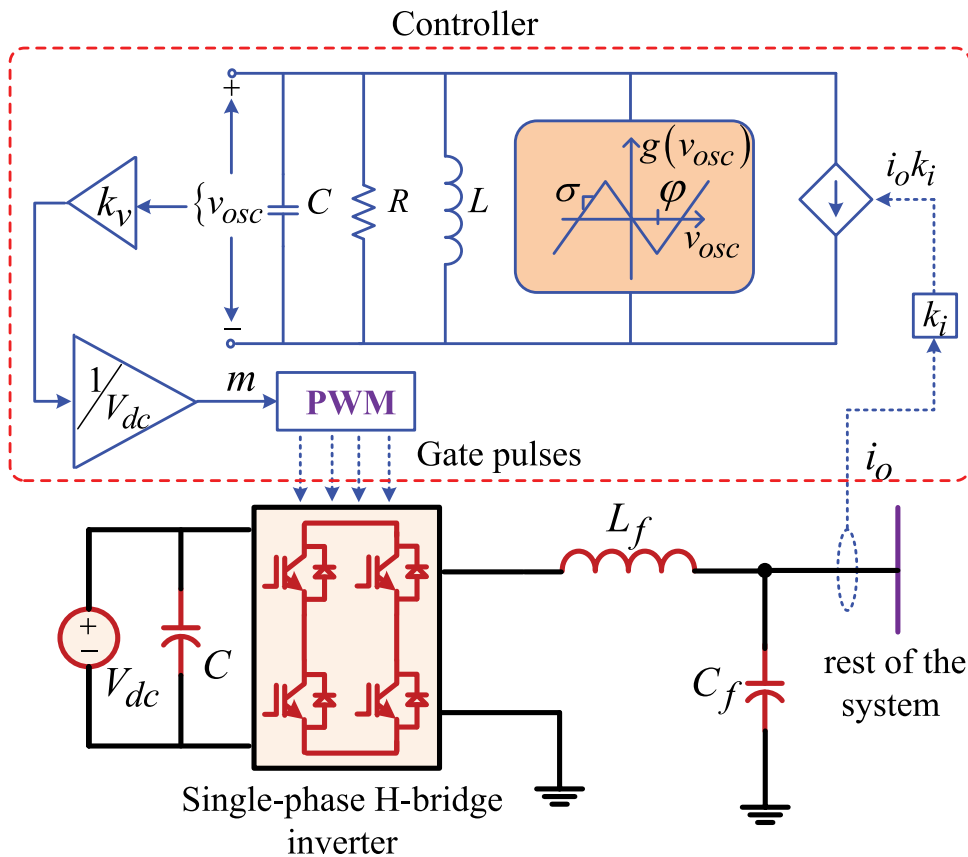


Figure 3. Single-Phase inverter with Dz-VOC.

Figure 3 shows the single-phase inverter with a Dz-VOC controller. By applying KCL and KVL to the Dz-VOC control, can get the dynamics of the states are shown in (3).

$$\frac{dv_{osc}}{dt} = \frac{1}{C} \left[\left(\sigma - \frac{1}{R} \right) v_{osc} - f(v_{osc}) - i_L - k_i i_0 \right]; \frac{di_L}{dt} = \frac{v_{osc}}{L} \quad (3)$$

To satisfy the global asymptotic synchronization requirement, all of the inverters in a parallel system that are tied to the same load need to have their terminal voltages synchronized. The synchronization condition is depicted in (4) as follows:

$$\max_{\omega \in R} \left\| \frac{(k_v k_i)^{-1} Z_f(j\omega) Z_{osc}(j\omega)}{(k_v k_i)^{-1} Z_f(j\omega) + Z_{osc}(j\omega)} \right\| \sigma < 1 \quad (4)$$

The synchronization condition includes several properties that are particularly intriguing. From (4), it is possible to ensure that synchronization in the system is maintained even though no information on the load side and how many inverters are joined. The design parameters of the Dz-VOC are presented in [Johnson et al. 2014].

To accommodate the power sharing of the inverters that are functioning in the system, the values of k (where k is a constant) are selected in a manner that is proportional to the inverter power ratings [Johnson et al. 2014]. In this instance, the x^{th} and y^{th} inverters, each of which has a power rating of P_x and P_y correspondingly. It is possible to demonstrate that if k_x and k_y are chosen in such a way that

$$\frac{P_x}{k_x} = \frac{P_y}{k_y} \quad x, y = 1, \dots, N, \quad (5)$$

Van der Pol oscillator based VOC

The VdP oscillator is a well-known approach for simulating non-linear dynamics in virtual oscillator control. A second-order oscillator model is used to describe this oscillator. Figure 4 depicts an SPI that is controlled by VdP oscillator controller. Harmonic oscillator with inductance and capacitance of the control circuit L and C , correspondingly, a negative-conductance ρ and a cubic VDCS $i_s(t)$ are the components that make up this oscillator control. The current that is drawn from the cubic VDCS can be calculated using the formula is αv_{osc}^3 , where α is a positive constant and v_{osc} is the oscillator state variable representing the virtual capacitance voltage. Another state variable, virtual inductance current i_L , can demonstrate the dynamics of an oscillator. The dynamic equation of the Van der Pol oscillator can be described as such if these variables are taken into account as shown in Equation (6)

$$\frac{dv_{osc}}{dt} = \frac{1}{C} [\rho v_{osc} - i_L - i_s(t) - i_0 k_i]; \frac{di_L}{dt} = \frac{v_{osc}}{L} \quad (6)$$

where $i_s(t) = \alpha v_{osc}^3$ and $\rho = -1/R$.

Design and parameter selection of Van del pol VOC

Equations found in [Johnson et al. 2016] are used as a reference in the process of designing the parameters of the VdP-VOC. Using the equations (7–12) mentioned below, the VdP-VOC parameters can be designed to meet a specific requirement.

$$k_v = V_{max}, k_i = \frac{V_{min}}{P_{rated}} \quad (7)$$

$$\alpha = \frac{2\rho}{3}, \rho = \frac{V_{max}}{V_{min}} \frac{V_{max}^2}{V_{max}^2 - V_{min}^2} \quad (8)$$

$$\max\{C_{min1}, C_{min2}\} \leq C_2 \leq C_{max} \quad (9)$$

$$C_{min1} = \frac{1}{2|\Delta\omega|_{max}} \frac{V_{max}}{V_{min}} \frac{Q_{rated}}{P_{rated}} \quad (10)$$

$$C_{min2} = \frac{\rho}{8} \frac{1}{\omega^* \delta_{3:1}^{max}} \quad (11)$$

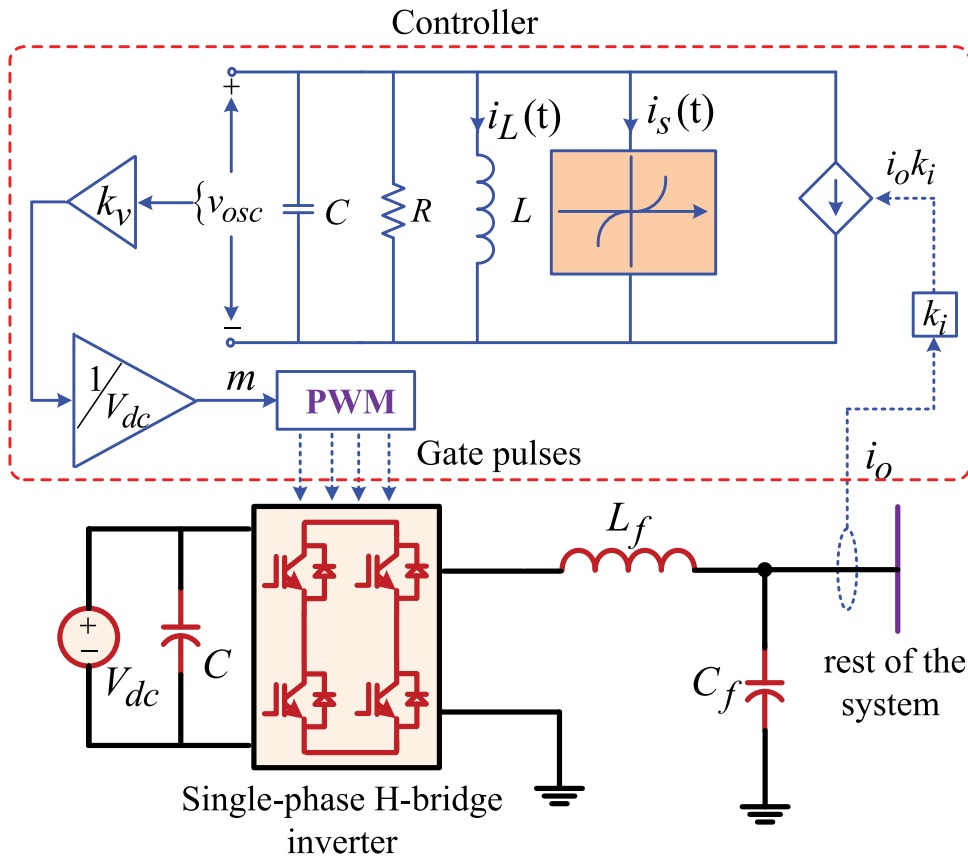


Figure 4. Single-Phase inverter with VdP-VOC.

$$C_{\max} = \frac{\rho}{6} t_{rise}^{\max} \quad (12)$$

where, V_{\max} and V_{\min} are the open-circuit voltage and voltage at rated power, respectively. P_{rated} and Q_{rated} are the rated real and reactive powers. ω^* is the nominal system frequency, $|\Delta\omega|_{\max}$ is the maximum frequency offset, $\delta_{3:1}^{\max}$ is the ratio of the 3rd to first harmonic, and t_{rise}^{\max} is the rise time of the system.

New virtual oscillator control and its characteristics

A new VOC is presented in this section. This new VOC can be achieved by making the NCS of the oscillator more efficient. Therefore, it is possible to attain superior synchronization and reduction in 3-order harmonic component in its output.

New virtual oscillator control

The nonlinear VDCS of a conventional VdP-VOC is a cubic-function of capacitor voltage, as shown in (13).

$$i_s(t) = \alpha v_{osc}^3 = 2\sqrt{2}\alpha V^3 \times \cos^3(\omega t + \theta) \quad (13)$$

The following result can be derived by using trigonometric identities:

$$\cos^3(z) = \frac{3}{4}\cos(z) + \frac{1}{4}\cos(3z) \quad (14)$$

Since the 3rd harmonic voltage is caused by $\cos(3z)$, it is not taken into consideration when creating a nonlinear current source based on (13). As a result, the oscillator's nonlinear current source can be altered to

$$i_s(t) = \alpha v_{osc}^3 = 2\sqrt{2}\alpha V^3 \times \frac{3}{4}\cos(z) = \frac{3}{2}\alpha V^2 \times v_{osc} \quad (15)$$

When (15) is placed in the place of (6), the result is

$$C \frac{d^2 v_{osc}}{dt^2} = -\frac{3}{2}\alpha V^2 \times \frac{dv_{osc}}{dt} + \rho \frac{dv_{osc}}{dt} - \frac{di_L}{dt} - k_i \frac{di_o}{dt} \quad (16)$$

The new VOC inductor current and an oscillator output voltage can be predicted using the equivalent circuit depicted in Figure 5.

$$\frac{di_L}{dt} = \frac{v_{osc}}{L} \quad (17)$$

$$\frac{dv_{osc}}{dt} = \frac{1}{C} \left[\left(-\frac{3}{2}\alpha V^2 \times v_{osc} \right) + \rho v_{osc} - i_L - i_0 k_i \right] \quad (18)$$

The oscillator output voltage is given by

$$v_{osc} = \sqrt{2}V \cos(\omega t + \theta) \quad (19)$$

When (19) is placed in the place of (17), the result is

$$\epsilon i_L = \sqrt{2}V \sin(\omega t + \theta) \quad (20)$$

The coordinate transformation is the next step to getting the (21)

$$\sqrt{2}V = \sqrt{(\epsilon i_L)^2 + v_{osc}^2} \quad (21)$$

However, it should be noted that in digital control, a new VOC is implemented using a new mathematical model shown in (17 and 18).

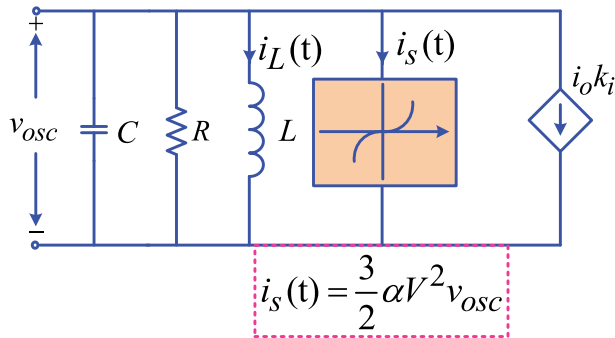


Figure 5. New VOC schematic diagram.

Elimination of 3rd order harmonic component in its output voltage

In this section, the harmonics of the suggested new VOC is investigated using a variety of scales and perturbation techniques [Luo et al. 2021]. Equation (16) can be reorganized in the time-coordinates $\tau = \omega^* t$ if we consider the scenario in which there is a VO that is not coupled to the inverter.

$$\frac{d^2 v_{osc}}{dt^2} - \varepsilon \left(\rho - \frac{3}{2} \alpha V^2 \right) \frac{dv_{osc}}{dt} + v_{osc} = 0 \quad (22)$$

where $\varepsilon \rightarrow 0$

It is reasonable to assume that, with the help of a regular perturbation expansion, the approximate solution to (22) can be broken down into the sum of its components based on some different time scales.

$$v_{osc}(\tau_0, \varepsilon) \approx v_x(\tau_0, \tau_1) + \varepsilon v_y(\tau_0, \tau_1) \quad (23)$$

where τ_0 is the original time-scale and $\tau_1 = \varepsilon \tau_0$ is the relaxed time-scale.

When (23) is placed in the place of (22), the result is

$$\left(\frac{\partial^2 v_x}{\partial \tau_0^2} + v_x \right) + \varepsilon \left(\frac{\partial^2 v_y}{\partial \tau_0^2} + v_y + 2 \frac{\partial^2 v_x}{\partial \tau_0 \partial \tau_1} - \rho \left(1 - \frac{3}{2} \alpha V^2 \right) \frac{\partial v_x}{\partial \tau_0} \right) = 0. \quad (24)$$

It is necessary that the terms in brackets $(\frac{\partial^2 v_x}{\partial \tau_0^2} + v_x = 0)$ are equal to 0 for the equation to be valid.

$$v_x(\tau_0, \tau_1) = a(\tau_1) \cos(\tau_0 + \theta(\tau_1)) \quad (25)$$

where $a(\tau_1)$ and $\theta(\tau_1)$ are the voltage amplitude and phase terms, respectively, and v_x is the oscillator fundamental component.

When (26) is placed in the place of (25), the result is

$$\frac{\partial^2 v_y}{\partial \tau_0^2} + v_y = \left(2 \frac{\partial a(\tau_1)}{\partial \tau_1} - \rho a(\tau_1) + \frac{3 \alpha V^2 a(\tau_1)}{2} \right) \sin(\tau_0 + \theta(\tau_1)) + 2a \frac{\partial \theta(\tau_1)}{\partial \tau_1} \cos(\tau_0 + \theta(\tau_1)). \quad (26)$$

In the conventional VOC, the lower time scales of v_y are written like this [Luo et al. 2021]:

$$\begin{aligned} \frac{\partial^2 v_y}{\partial \tau_0^2} + v_y &= \left(2 \frac{\partial a(\tau_1)}{\partial \tau_1} - \rho a(\tau_1) + \frac{\rho}{2} a^3(\tau_1) \right) \sin(\tau_0 + \theta(\tau_1)) + 2a(\tau_1) \frac{\partial \theta(\tau_1)}{\partial \tau_1} \cos(\tau_0 + \theta(\tau_1)) \\ &\quad + \frac{\rho}{2} a^3(\tau_1) \sin(3\tau_0 + 3\theta(\tau_1)) \end{aligned} \quad (27)$$

Because of this, the estimated solution on smaller time-scales in the suggested new VOC does not include the 3rd order harmonic term. This can be deduced from (26) and (27), which state that the NCS of the oscillator can be changed to eliminate the 3rd harmonic term.

The suggested VOC v_y value can be obtained as follows:

$$v_y = a_1 \cos(\tau_1 + \theta_1) \quad (28)$$

and the conventional VOC's v_y value is given by

$$v_y = -\frac{\rho}{4\sqrt{\beta}} \sin(3\tau_0 + \theta_0). \quad (29)$$

Equations 28, 29) suggest that the undesirable 3rd order harmonic term will not be present in the suggested new VOC, although it is present in the conventional VdP-VOC. Considering that τ_1 is the slower time-scale, the proposed new VOC term v_y has a negligible impact on the steady-state solution of v_{osc} .

Simulation results and discussion

Three SPIs are joined in parallel in the simulation model's architecture, and each inverter is interfaced with a DC source. Simulations are accompanied for the islanded MG system as shown in Figure 1. Different types of loads (Resistive Load, Linear RLC load, and Nonlinear load) are used in this simulation study are shown in Figure 6. Three inverters are connected in parallel and run in islanded mode in the system under different load considerations. The virtual oscillators associated with each inverter were initialized such that $v(0) = [0.2 \text{ V}; 0.22 \text{ V}; 0.24 \text{ V}]^T$.

Case (i): (Resistive load)

Here, the load is resistive as shown in Figure 6(a) and the inverters are set up with uniform power sharing (1:1:1). Figures 7, 8, and 9 show the current sharing and voltage synchronization of the inverters in Dz-VOC, VdP-VOC, and new VOC controllers, respectively, in an equal (1:1:1) and unequal (2:2:1) power sharing with resistive load. The step change in load occurred at 0.6 s, the inverters increase their output currents almost instantaneously in all the controllers. During start-up, the synchronization is very quick in Dz-VOC and new VOC controllers compared to VdP-VOC.

Case (ii): (Linear RLC load)

Here, the load is a Linear RLC circuit as shown in Figure 6(b) and the inverters are set up with both uniform (1:1:1) and non-uniform (2:2:1) power sharing. Figures 10(a,b), 11(a,b), and 12(a,b) show the current sharing and voltage-synchronization of the SPIs in Dz-VOC, VdP-VOC, and new VOC controllers, respectively, in an equal (1:1:1) power sharing with linear RLC load. At 0.6 s, there is a step change in the load, and all of the controllers' inverters raise their output currents almost instantly. When the Dz-VOC and new VOC controllers startup, synchronization happens very quickly. In the case of unequal (2:2:1) power sharing, Figures 10(c,d), 11(c,d), and 12(c,d) show how the inverters share current and synchronize voltage in the Dz-VOC, VdP-VOC, and new VOC controllers, respectively, in the case of unequal (2:2:1) power sharing.

Case (iii): (Nonlinear load)

Here, the load is nonlinear as shown in Figure 6(c) and the inverters are set up with both uniform (1:1:1) and non-uniform (2:2:1) power sharing. Figures 13(a,b), 14(a,b), and 15(a,b) show the current sharing and voltage-synchronization of the SPIs in Dz-VOC, VdP-VOC, and new VOC controllers, respectively, in the case of equal (1:1:1) power sharing. Synchronization occurs rapidly in the Dz-VOC and new VOC controllers during start-up. Figures 13(c,d), 14(c,d), and 15(c,d) show how the inverters share current and synchronize voltage in the Dz-VOC, VdP-VOC, and new VOC controllers, respectively, in the case of unequal (2:2:1) power sharing.

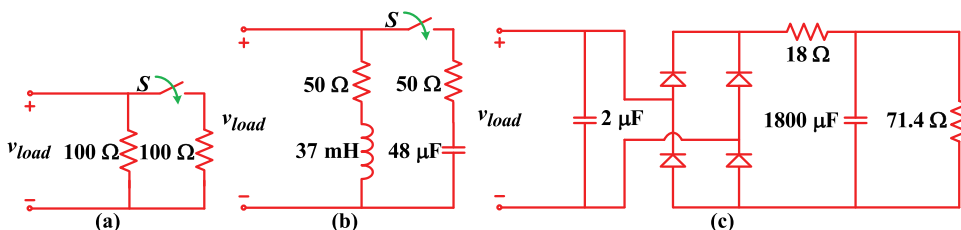


Figure 6. (a) Resistive load, (b) linear RLC load, (c) nonlinear load.

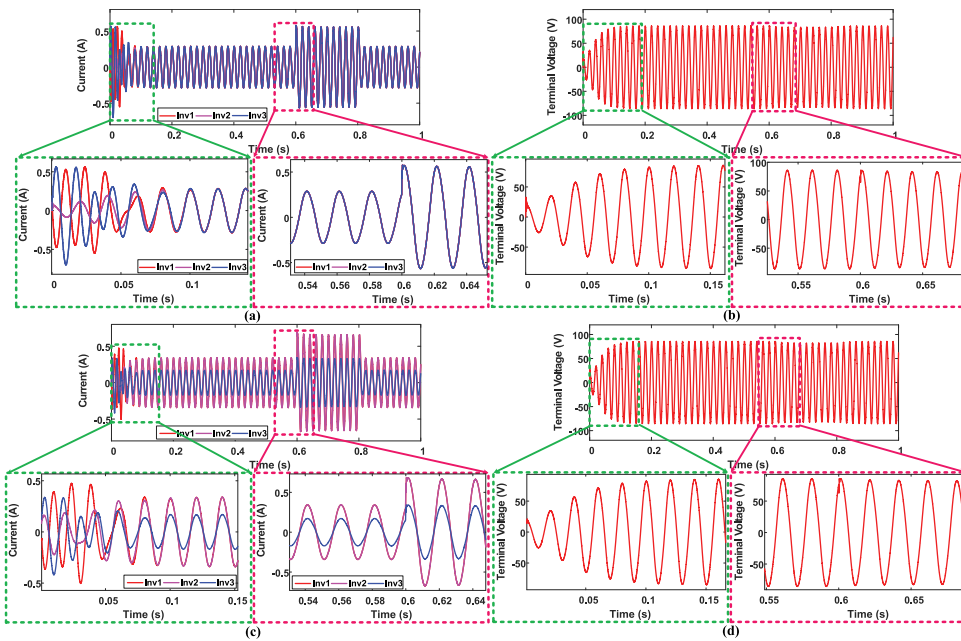


Figure 7. Dzo controller-Resistive load (a) Current sharing (b) Voltage synchronization (1:1:1 power sharing) and (c) Current sharing (d) Voltage synchronization (2:2:1 power sharing).

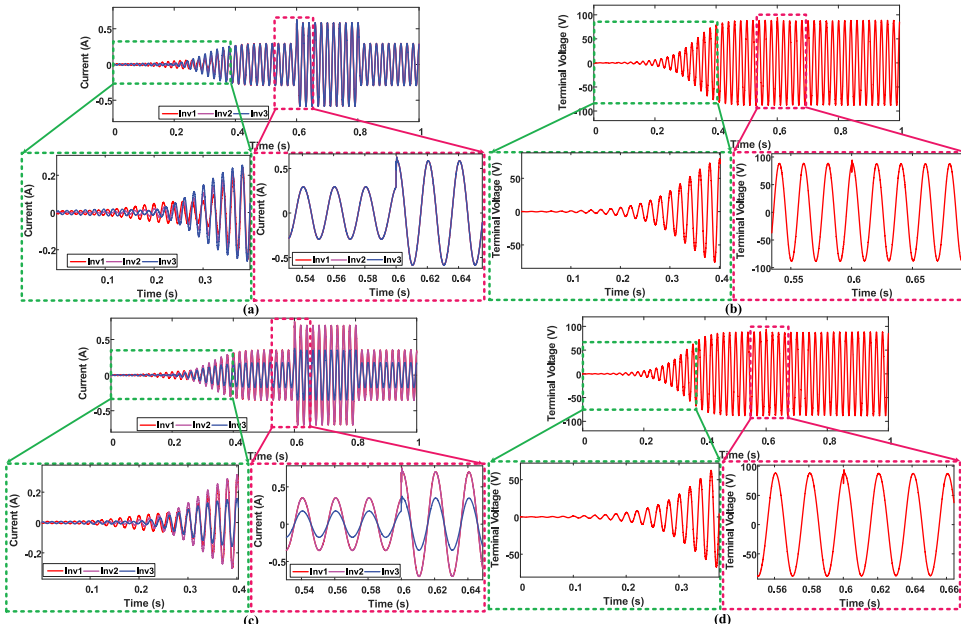


Figure 8. VPO controller-Resistive load (a) Current sharing (b) Voltage synchronization (1:1:1 power sharing) and (c) Current sharing (d) Voltage synchronization (2:2:1 power sharing).

THD analysis

The THD of the current in Dz-VOC, VdP-VOC, and new VOC are 1.98%, 1.11%, and 0.21%, respectively, with linear RLC load. The 3rd harmonic is dominant in both Dz and VdP VOCs, while in the new VOC the 3rd harmonic is very less and below 0.1%. The THD of the current in the

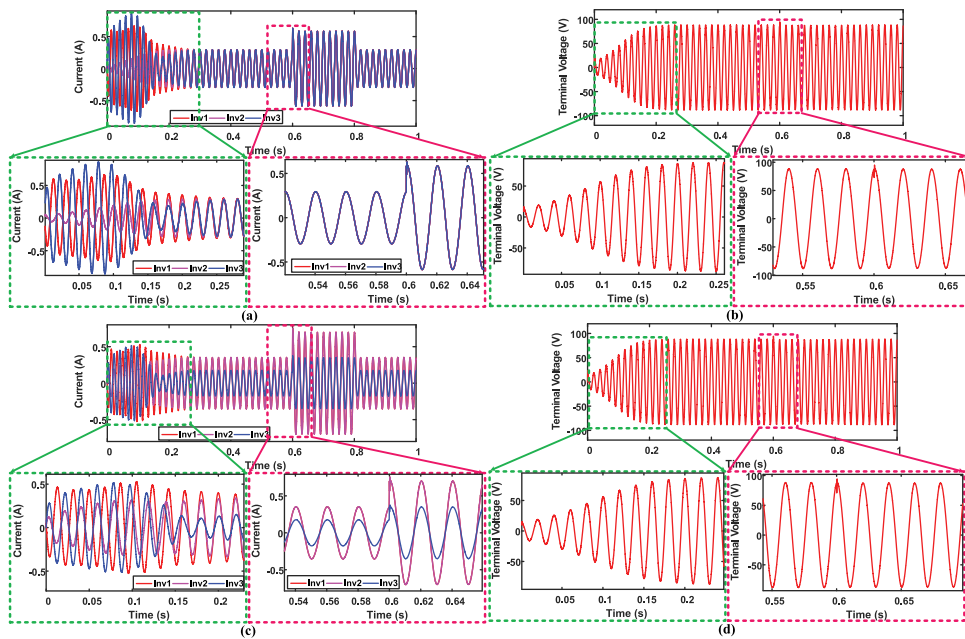


Figure 9. Modified VPO controller-Resistive load (a) Current sharing (b) Voltage synchronization (1:1:1 power sharing) and (c) Current sharing (d) Voltage synchronization (2:2:1 power sharing).

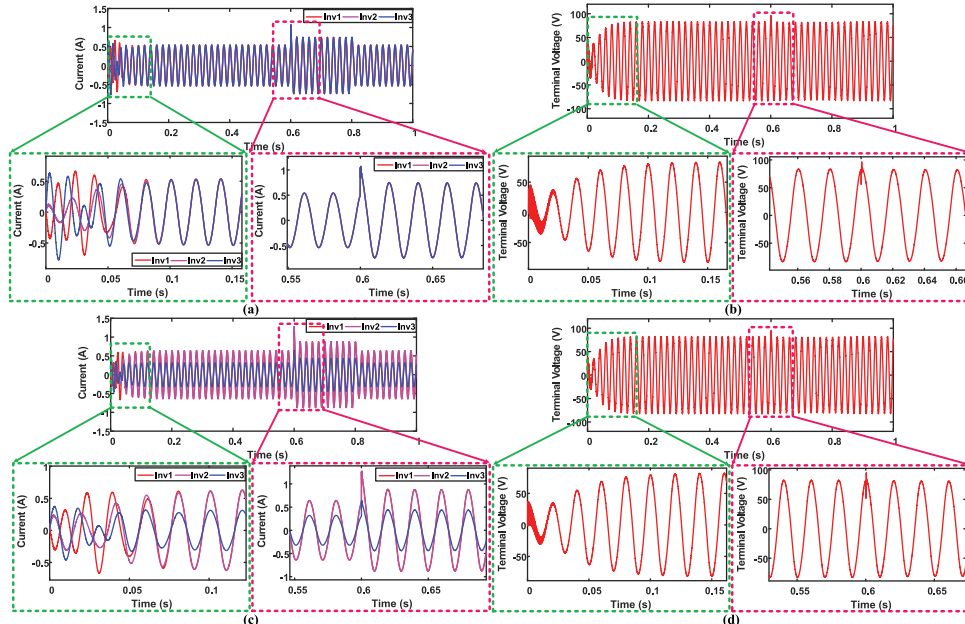


Figure 10. Dzo controller-Linear RLC load (a) Current sharing (b) Voltage synchronization (1:1:1 power sharing) and (c) Current sharing (d) Voltage synchronization (2:2:1 power sharing).

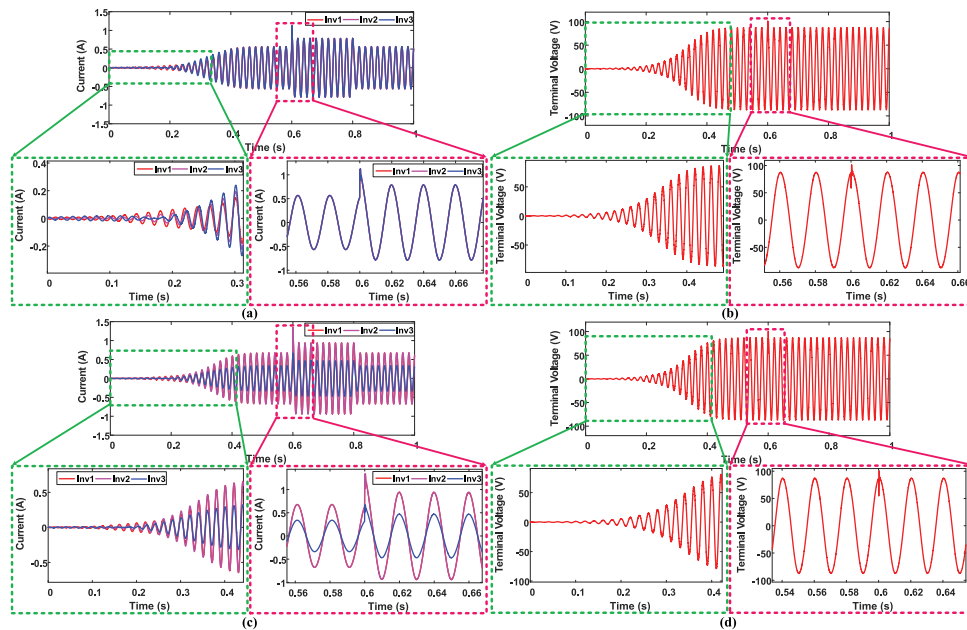


Figure 11. VPO controller-Linear RLC load (a) Current sharing (b) Voltage synchronization (1:1:1 power sharing) and (c) Current sharing (d) Voltage synchronization (2:2:1 power sharing).

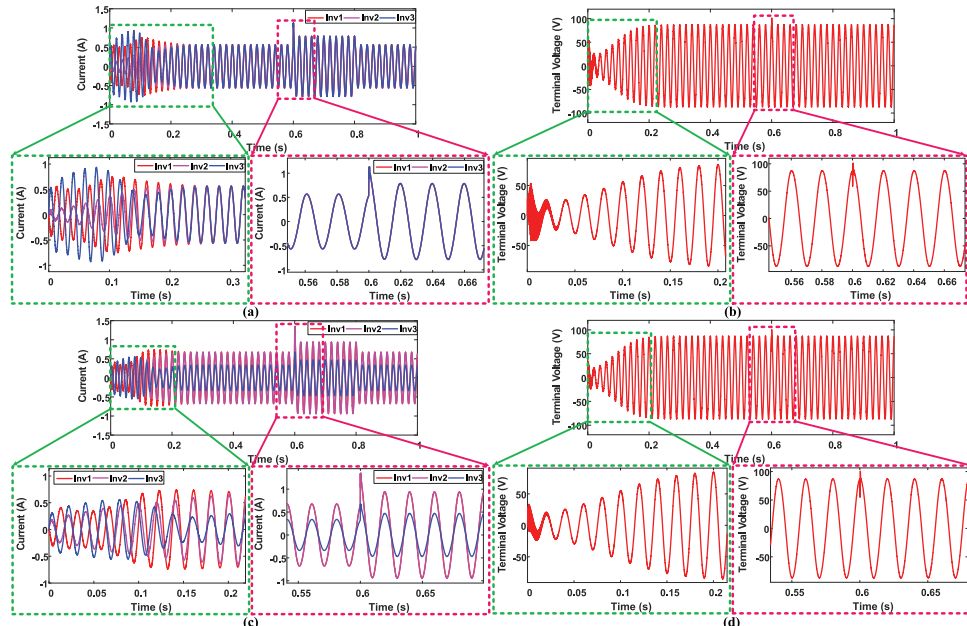


Figure 12. Modified VPO controller-Linear RLC load (a) Current sharing (b) Voltage synchronization (1:1:1 power sharing) and (c) Current sharing (d) Voltage synchronization (2:2:1 power sharing).

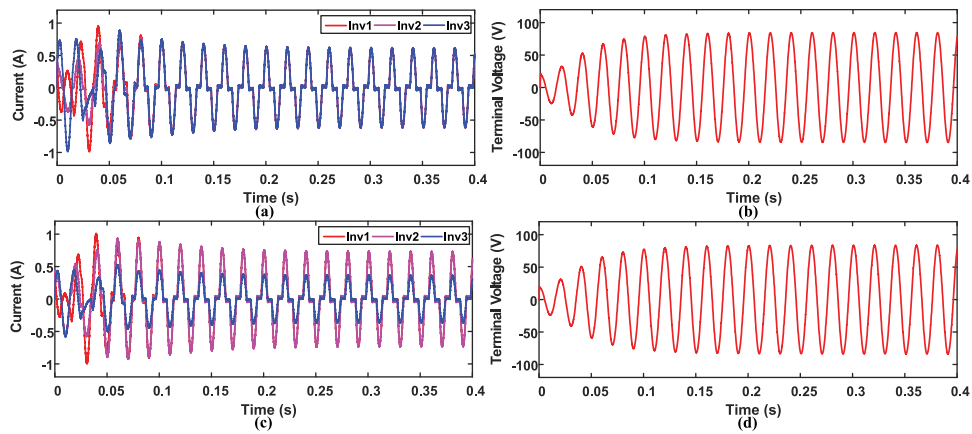


Figure 13. Dzo controller-Nonlinear load (a) Current sharing (b) Voltage synchronization (1:1:1 power sharing) and (c) Current sharing (d) Voltage synchronization (2:2:1 power sharing).

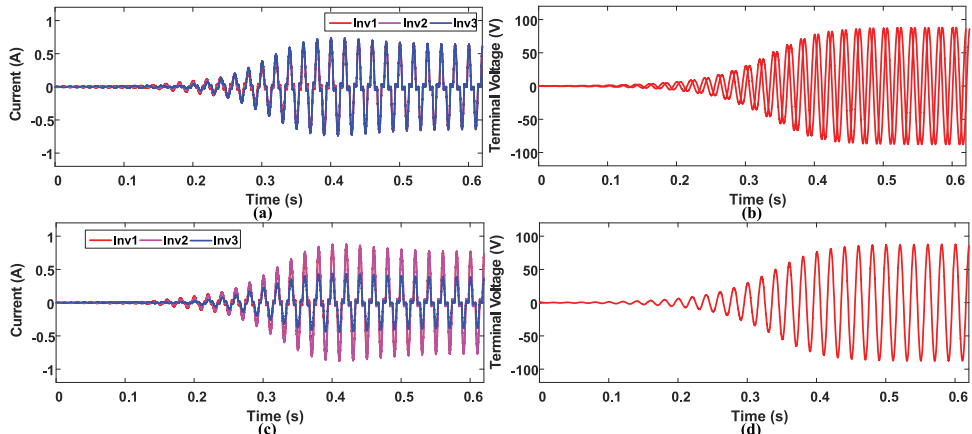


Figure 14. VPO controller-Nonlinear load (a) Current sharing (b) Voltage synchronization (1:1:1 power sharing) and (c) Current sharing (d) Voltage synchronization (2:2:1 power sharing).

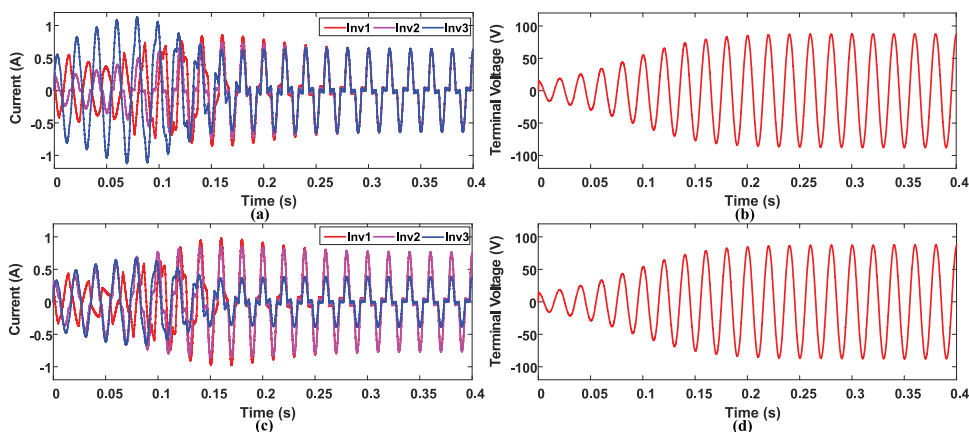


Figure 15. Modified VPO controller-Nonlinear load (a) Current sharing (b) Voltage synchronization (1:1:1 power sharing) and (c) Current sharing (d) Voltage synchronization (2:2:1 power sharing).

abovementioned controllers is shown in Figs. 16(a, c, e), respectively. The THD of the voltage in the abovementioned controllers is 2.35%, 1.31%, and 1.54%, and shown Figs. 16(b, d, f), respectively. Finally, the 3rd harmonic component in THD is very less in new VOC compared to other controllers.

Hardware results and discussion

A new VOC control method is used for SPI operation. Each of the aforementioned control strategies is being demonstrated through simulation investigation. Finally, hardware implementation and its

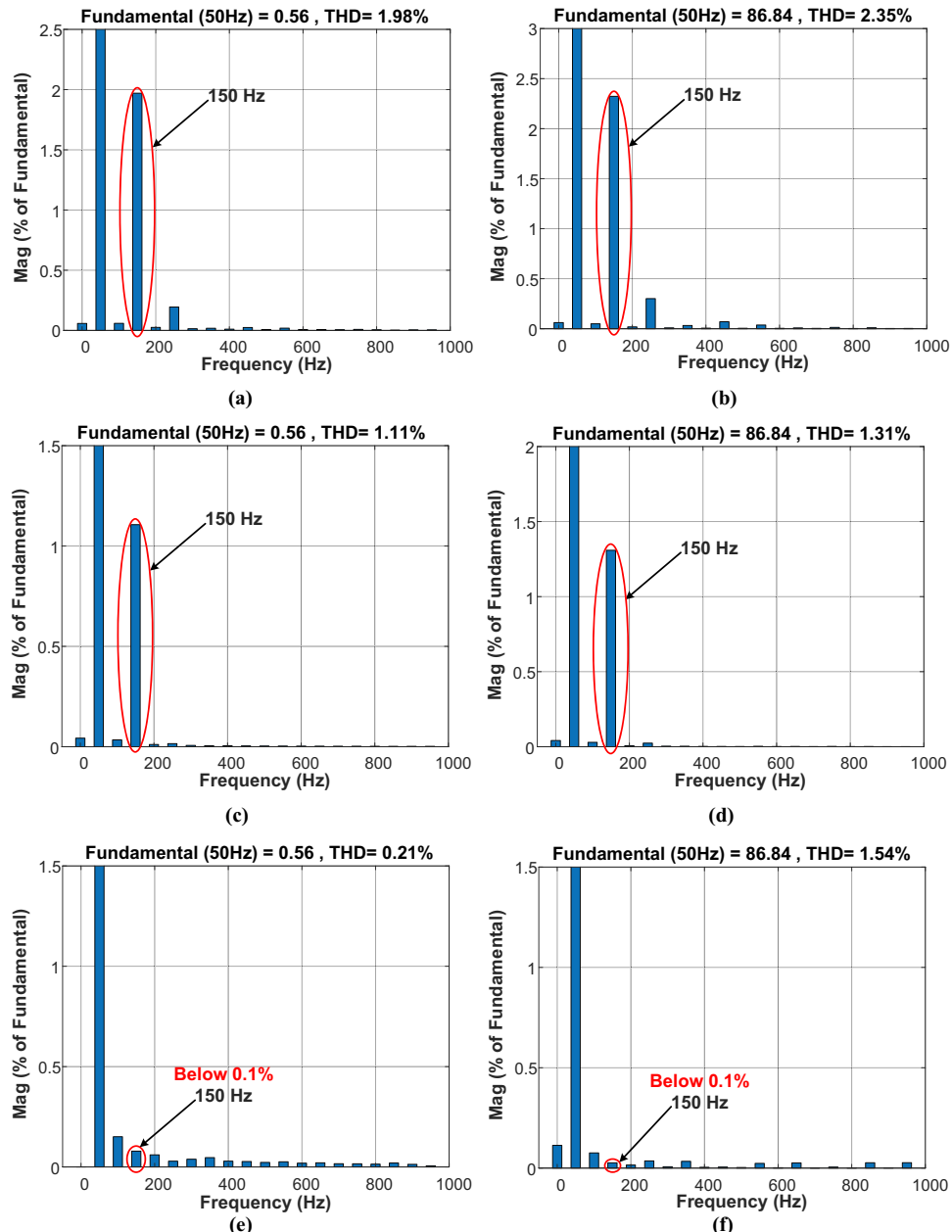


Figure 16. THD in Dz-VOC (a) Current (b) Voltage; THD in VdP-VOC (c) Current (d) Voltage; THD in New VOC (e) Current (f) Voltage.

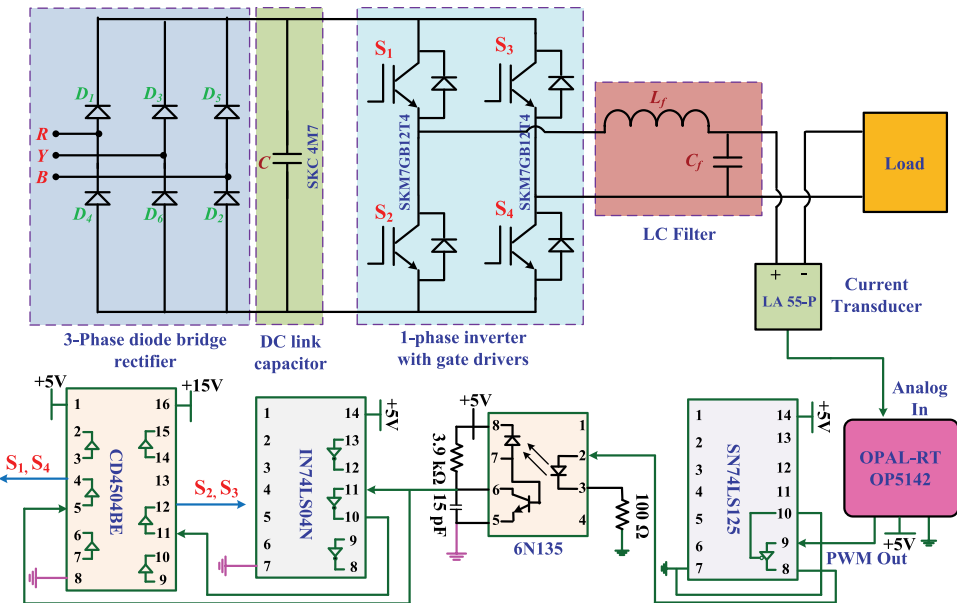


Figure 17. Experimental model diagram.

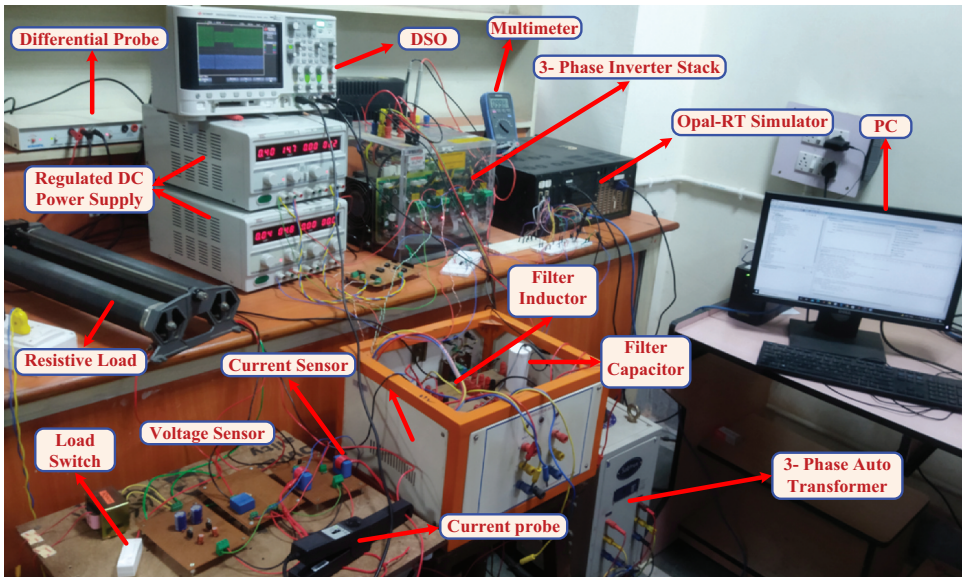


Figure 18. Experimental setup.

validation of the new VOC control technique have been accomplished. An SPI experimental model circuit diagram is shown in Figures 17 and 18 shows the experimental setup.

Figure 19(a) shows the transient response of the inverter output voltage and current with repetitive step changes in the resistive load (54Ω to 27Ω and 27Ω to 54Ω) with new VOC control. Figure 19(b & c) show the dynamic response of the inverter with step-up and step-down changes in a resistive load, correspondingly.

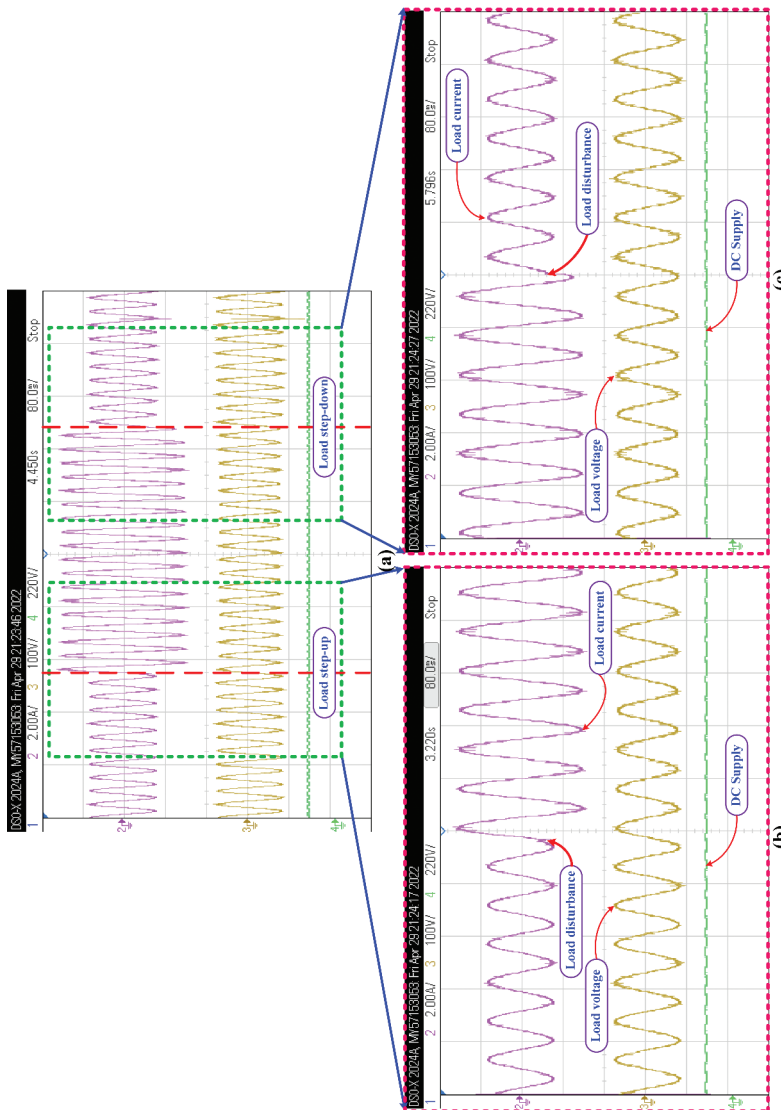


Figure 19. Transient response of the inverter output voltage and current with new VOC (a) with repetitive step changes in the load (b) with step-up change in load (c) with step-down change in load.

Conclusion

This paper offers two well-known VOCs and a new VOC for parallel inverters. The current sharing and voltage synchronization of parallel inverters is standalone MG with Dz-VOC, VdP-VOC, and new VOC-based controllers are presented. Three different types of loads (Resistive load, Linear RLC load, and nonlinear load) applied in this system. In this, the authors presented an extensive comparison of Dz-VOC, VdP-VOC, and new VOC-based controllers. In comparison to the conventional VdP-VOC controller, the new VOC-based controller reduces harmonic distortion and achieves a quicker transient response. The simulation and hardware results demonstrate the effectiveness of the control strategy based on the new VOC. Furthermore, intelligent methods such as model predictive control (MPC) and artificial intelligence (AI) can be integrated with VOC to enhance its performance and facilitate its implementation in large-scale systems.

Nomenclature

VOC	Virtual oscillator control
SPI	Single-phase inverter
MG	Microgrid
NCS	Non-linear current source
Dz-VOC	Deadzone based VOC
VdP-VOC	Van der pol based VOC
LPF	Low pass filter
KCL	Kirchhoff's current law
KVL	Kirchhoff's voltage law
VDCS	Voltage dependent current source
THD	Total harmonic distortion
MPC	Model predictive control
AI	Artificial intelligence.

Acknowledgments

The idea of work is supported by DST project Scheme for Young Scientists and Technologists (SP/YO/2019/1349).

Disclosure statement

No potential conflict of interest was reported by the author(s).

References

- Awal, M., H. Yu, I. Husain, W. Yu, and S. Lukic. 2020. Selective harmonic current rejection for virtual oscillator controlled grid-forming voltage source converters. *IEEE Transactions on Power Electronics* 35(8): Aug. 8805–18. doi:[10.1109/TPEL.2020.2965880](https://doi.org/10.1109/TPEL.2020.2965880).
- Awal, M., H. Yu, H. Tu, S. M. Lukic, and I. Husain. 2020. Hierarchical control for virtual oscillator based grid-connected and islanded microgrids. *IEEE Transactions on Power Electronics* 35(1): Jan. 988–1001. doi:[10.1109/TPEL.2019.2912152](https://doi.org/10.1109/TPEL.2019.2912152).
- De Brabandere, K., B. Bolsens, J. Van den Keybus, A. Woyte, J. Driesen, and R. Belmans. 2007. A voltage and frequency droop control method for parallel inverters. *IEEE Transactions on Power Electronics* 22(4): Jul. 1107–15. doi:[10.1109/TPEL.2007.900456](https://doi.org/10.1109/TPEL.2007.900456).
- Dhople, S., B. Johnson, F. Dörfler, and A. Hamadeh. 2014. Synchronization of nonlinear circuits in dynamic electrical networks with general topologies. *IEEE Transactions on Circuits and Systems I: Regular Papers* 61(9): Sep. 2677–90. doi:[10.1109/TCSI.2014.2332250](https://doi.org/10.1109/TCSI.2014.2332250).



- Dhopole, S. V., B. B. Johnson, and A. O. Hamadeh, "Virtual oscillator control for voltage source inverters," in 2013 51st Annual Allerton Conference on Communication, Control, and Computing (Allerton), pp. 1359–63, Oct. 2013. doi:10.1109/Allerton.2013.6736685.
- Guerrero, J. M., P. C. Loh, T.-L. Lee, and M. Chandorkar. 2013. Advanced control architectures for intelligent microgrids—part II: Power quality, energy storage, and AC/DC microgrids. *IEEE Transactions on Industrial Electronics* 60(4): Apr. 1263–70. doi:10.1109/TIE.2012.2196889.
- Hansen, K., C. Breyer, and H. Lund. 2019. Status and perspectives on 100% renewable energy systems. *Energy* 175: 471–80. doi: 10.1016/j.energy.2019.03.092.
- Johnson, B. B., S. V. Dhopole, A. O. Hamadeh, and P. T. Krein. 2014. Synchronization of nonlinear oscillators in an LTI electrical power network. *IEEE Transactions on Circuits and Systems I: Regular Papers* 61(3): Mar. 834–44. doi:10.1109/TCSI.2013.2284180.
- Johnson, B. B., S. V. Dhopole, A. O. Hamadeh, and P. T. Krein. 2014. Synchronization of parallel single-phase inverters with virtual oscillator control. *IEEE Transactions on Power Electronics* 29(11): Nov. 6124–38. doi: 10.1109/TPEL.2013.2296292.
- Johnson, B., M. Rodriguez, M. Sinha, and S. Dhopole, "Comparison of virtual oscillator and droop control," in Proc. IEEE 18th Workshop Control Model. Power Electron. 2017, pp. 1–6. doi:10.1109/COMPEL.2017.8013298.
- Johnson, B., M. Sinha, N. Ainsworth, F. Dörfler, and S. Dhopole. 2016. Synthesizing virtual oscillators to control islanded inverters. *IEEE Transactions on Power Electronics* 31(8): Aug. 6002–15. doi: 10.1109/TPEL.2015.2497217.
- Liu, J., Y. Miura, H. Bevrani, and T. Ise. 2017. Enhanced virtual synchronous generator control for parallel inverters in microgrids. *IEEE Transactions on Smart Grid* 8(5): Sep. 2268–77. doi: 10.1109/TSG.2016.2521405.
- Lu, M., S. Dutta, and B. Johnson. 2022. Self-Synchronizing cascaded inverters with virtual oscillator control. *IEEE Transactions on Power Electronics* 37(6): Jun. 6424–36. doi:10.1109/TPEL.2021.3134662.
- Luo, S., W. Wu, E. Koutroulis, H. S. H. Chung, and F. Blaabjerg. 2021. A new virtual oscillator control without third-harmonics injection for DC/AC inverter. *IEEE Transactions on Power Electronics* 36(9): Mar. 10879–88. doi:10.1109/TPEL.2021.3066162.
- Luo, S., W. Wu, E. Koutroulis, H. S. H. Chung, and F. Blaabjerg. 2022. A New Kalman-Filter-Based Harmonic Current Suppression Method for the Virtual Oscillator Controlled Grid-Tied Inverter. *IEEE Journal on Emerging and Selected Topics in Circuits and Systems* 12(1): Jan. 251–59. doi:10.1109/JETCAS.2022.3141106.
- Lu, M., G. Seo, M. Sinha, F. Rodriguez, S. Dhopole, and B. Johnson, "Adaptation of commercial current-controlled inverters for operation with virtual oscillator control," in Proc. IEEE Appl. Power Electron. Conf. Expo. Mar. 2019, pp. 3427–32. doi:10.1109/APEC.2019.8722234.
- Raisz, D., T. T. Thai, and A. Monti. 2019. Power control of virtual oscillator controlled inverters in grid-connected mode. *IEEE Transactions on Power Electronics* 34(6): Jun. 5916–26. doi:10.1109/TPEL.2018.2868996.
- Rocabert, J., A. Luna, F. Blaabjerg, and P. Rodriguez. 2012. Control of power converters in AC microgrids. *IEEE Transactions on Power Electronics* 27(11): Nov. 4734–49. doi:10.1109/TPEL.2012.2199334.
- Sinha, M., F. Dörfler, B. B. Johnson, and S. V. Dhopole. 2017. Uncovering droop control laws embedded within the nonlinear dynamics of Van der Pol oscillators. *IEEE Transactions on Control of Network Systems* 4(2): Jun. 347–58. doi:10.1109/TCNS.2015.2503558.
- Strogatz, S. 2012. *Sync: How Order Emerges from Chaos in the Universe, Nature, and Daily Life*. New York, USA: Hyperion.
- Tôrres, L. A., J. Hespanha, and J. Moehlis, "Power supply synchronization without communication," in Proc. IEEE Power Energy Soc. Gen. Meeting, 2012, pp. 1–6. doi:10.1109/PESGM.2012.6344905.
- Zhong, Q. C., and G. Weiss. 2011. Synchronverters: Inverters that mimic synchronous generators. *IEEE Transactions on Industrial Electronics* 58(4): Apr. 1259–67. doi:10.1109/TIE.2010.2048839.

Appendix

Simulation parameters:

System parameters: System voltage = 60 V (rms); frequency = 50 Hz; $L_f = 6 \text{ mH}$, $R_f = 1 \Omega$, $C_f = 1.2 \mu\text{F}$; DC supply = 100 V; switching frequency = 25 kHz.

Deadzone VOC parameters: Oscillator RLC parameters: $R = 10\Omega$, $L = 718.59 \mu\text{H}$, $C = 14.12 \text{ mF}$. Oscillator non-linear subsystem parameters: $\sigma = 1 \text{ S}$, $\varphi = 0.47 \text{ V}$. Voltage scaling factor and current scaling factor: $k_v = 84.85$, $k_i = 0.1125$.

Van der pol VOC parameters: Oscillator LC parameters: $L = 56.29 \mu\text{H}$, $C = 0.18 \text{ F}$. Conductance $\rho = 6.09 \text{ S}$, Oscillator non-linear parameter $\alpha = 4.06$, Voltage gain $k_v = 63$, and current gain $k_i = 0.57$.